Geol. Mag. **146** (*2*), *2009, pp. 161–172.* © *2008 Cambridge University Press*
doi:10.1017/S001675680800544X *Printed in the United Kingdom*

Age distribution of cinder cones within the Bandas del Sur Formation, southern Tenerife, Canary Islands

JÖRG KRÖCHERT & ELMAR BUCHNER*

Institut für Planetologie, Universität Stuttgart, Herdweg 51, 70174 Stuttgart, Germany

(*Received* 28 September 2007; *accepted* 11 April 2008; First published online 16 September 2008)

Abstract – The Quaternary Bandas del Sur Formation in the south of Tenerife comprises a complex sequence of pyroclastic rocks and lavas. In contrast to the NW- and NE-Rift zone on Tenerife, the S-Rift zone comprises a number of characteristics with respect to the morphological features, eruption cyclicity and the geochemistry of the volcanic deposits. Various flank eruptions of the Las Cañadas volcano associated with basaltic lavas and the formation of cinder cones within the Bandas del Sur are important volcanic units for understanding the explosive volcanic cycles during the Pleistocene on Tenerife. A number of palaeomagnetic studies, as well as major and trace element geochemistry and two radio-isotope dates (K–Ar), have been carried out on prominent cinder cones, in order to discover their stratigraphic position. Combining our results with previous K–Ar data, the cones and lavas can be subdivided into three stratigraphic units. The first unit contains cinder cones with reverse magnetization and Y/Nb ratios between 0.37 and 0.41. Cinder cones which belong to the second unit show normal magnetization and Y/Nb ratios of < 0.35. The third unit comprises cinder cones with normal magnetization and Y/Nb ratios of about 0.47. The first two units were constructed between *c*. 0.948–0.779 Ma and 0.323–0.300 Ma. These units define volcanic cycles ending in violent Plinian eruptions. The third and youngest unit possibly marks the beginning of a further volcanic cycle that started *c.* 0.095 Ma ago.

Keywords: cinder cones, Bandas del Sur, Tenerife, Canary Islands, palaeomagnetism, geochemistry.

1. Introduction

The Canary Islands are a group of ocean island volcanoes situated near the continental margin of northwest Africa. Tenerife is the largest and topographically highest island in the Canaries, with a base area of > 2000 km^2 and a summit elevation of 3718 m (Pico de Teide). The oldest volcanic rocks exposed on Tenerife are the remnants of the basalt shield massifs of Roque del Conde (S Tenerife), Anaga (NE Tenerife), and Teno (NW Tenerife; Fig. 1a), with a constructional age between 11.9 Ma and 3.9 Ma (Guillou *et al.* 2004*a*). Fuster *et al.* (1968) combined the volcanic rocks of these massifs into the Old Basaltic Series.

The Las Cañadas volcano in the central part of Tenerife started to grow more than 3 Ma ago (Fuster *et al.* 1994). The formations of the Las Cañadas volcano were divided into a Lower and an Upper Group (Fig. 1b) by Marti, Mitjavila & Araña (1994). The Lower Group was erupted between > 3 Ma (Fuster *et al.* 1994) and 2 Ma (Marti, Mitjavila & Araña, 1994) and comprises basaltic, phonolitic and trachytic lavas and subordinate pyroclastic rocks (Ancochea *et al.* 1990). The volcanic rocks of the Upper Group are dominated by pyroclastic deposits that have been erupted during cyclic explosive volcanic activity (Marti, Mitjavila & Araña, 1994).

The summit region of the Las Cañadas volcano is characterized by a large depression, known as the Las Cañadas caldera. The origin of this depression is still the subject of controversy; gravitational collapses resulting in giant landslides, vertical collapses caused by emptying of shallow magma chambers or a combination of vertical and lateral collapses are the most plausible processes (for detailed discussion, see Brown *et al.* 2003; Carracedo *et al.* 2007; Edgar *et al.* 2007). Inside the Las Cañadas caldera, the stratovolcanoes of Pico de Teide and Pico Viejo post-date the caldera forming Upper Group cycles, and have a constructional age of > 150 ka (Araña, Barberi & Ferrara, 1989).

Marti, Mitjavila & Araña (1994) subdivided the Upper Group into three explosive volcanic cycles: the Ucanca Formation (1.59–1.18 Ma), the Guajara Formation (0.85–0.65 Ma) and the Diego Hernández Formation (0.37–0.17 Ma). The Bandas del Sur Formation comprises more than seven widespread ignimbrite sheets erupted from the Las Cañadas edifice (Brown *et al.* 2003) during two explosive volcanic cycles (Cycle 2: > 0.76–0.57 Ma and Cycle 3: > 0.32–0.17 Ma; Bryan, Martí & Cas (1998); Fig. 1b). Each cycle is inferred to have started with flank eruptions of alkali basalt lava and the growth of cinder cones. Three widely eroded cinder cones, cropping out in the east of the Bandas del Sur (Fig. 1a), are all the remains of the basaltic eruptions at the initial phase of Cycle 2 (Bryan, Martí & Cas, 1998). The Cycle 3 basalts (Series III basalts of Fuster *et al.* 1968) are widely distributed within the Bandas del Sur. The youngest episode of flank eruptions within the Bandas del Sur resulted in the lavas and cinder cones of the

*Author for correspondence: elmar.buchner@geologie.uni-stuttgart.de

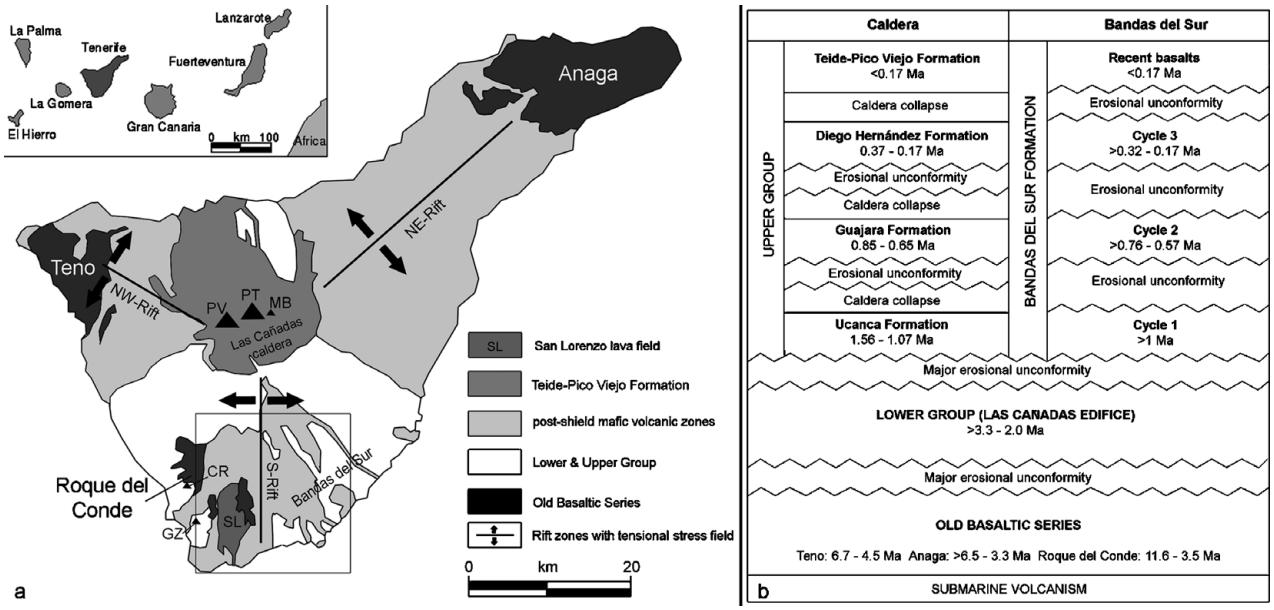

Figure 1. (a) Simplified geological map of Tenerife island, showing the main volcanic features; modified after Ablay & Martí (2000), Carracedo (1994) and Carracedo *et al.* (2007). Frame marks the study area (presented in detail in Fig. 2). CR – Caldera del Rey; GZ – Montaña Guaza; MB – Montaña Blanca; PT – Pico de Teide; PV – Pico Viejo; SL – San Lorenzo lava field. (b) Volcanic stratigraphy of Tenerife; modified after Bryan, Martí & Cas (1998).

San Lorenzo lava field (the Recent basalts *sensu* Bryan, Martí & Cas, 1998). These are equivalent to the Recent Series of Marti, Mitjavila & Araña (1994) and Series IV (Series Recientes IV e Historica) of Fuster *et al.* (1968). Each cycle evolved from initial basaltic to phonolitic eruptions (Bryan, Martí & Leosson, 2002). The aim of this study is to determine the stratigraphic position and age distribution of the cinder cones in the Bandas del Sur, using magnetic stratigraphy, geochemistry and K–Ar ages.

2. Methods

2.a. Palaeomagnetism

Palaeomagnetic studies were carried out on 44 cinder cones within the Bandas del Sur, using a modified version of the fluxgate magnetometer 'Fluxmaster' (Stefan-Mayer Instruments). Field measurements using a portable magnetometer have been successfully carried out in the Canary Islands (e.g. Carracedo, 1979; Guillou *et al.* 2004*a*, *b*; Paris *et al.* 2006). The magnetization of 85 % of the samples measured during field work has been identical with samples measured in laboratory (Guillou *et al.* 2004*b*). In a study by Doell & Cox (1962), the error margin of the samples measured in the field was about 5 % for volcanic rocks. Accordingly, a minimum of six measurements were carried out for each cinder cone, using orientated samples of the cores from large *in situ* volcanic bombs and/or samples of lava flows issued from the cones. The samples were collected over the entire extent of each cone, in order to obtain statistically viable results and to avoid local polarity reversals caused by lightning. For readability, the following terms are used: 'R-Basalts' for cones and lavas with reverse remanent magnetization, 'N-Basalts' for cones with normal remanent magnetization (except the younger cones of the San Lorenzo lava field) and 'N-Basalts-SL' for all cinder cones of the San Lorenzo lava field, owing to the fact that these cones invariably show normal remanent magnetization.

2.b. Geochemistry

Major and trace element concentrations have been determined for 16 whole-rock samples at the Institute of Mineralogy, University of Stuttgart, and at the IFM-GEOMAR, Kiel, by XRF methods (Table 1). After crushing they were pulverized using an automatic tungsten carbide mill. The analyses were carried out using a Rh-tube, calibrated by international geological standards. The CO_2 and H_2O concentrations were dissected by infrared photometry after the pulverized samples were heated up to 1000 °C.

2.c. K–Ar age dating

For the K–Ar age determination, unweathered samples were used. The age determinations were carried out for two samples at the Laboratoire des Sciences du Climat et l'Environment (France). The materials used were whole rock samples, crushed to particle sizes varying between 0.250 and 0.125 mm, and ultrasonically washed in $HC_2H_3O_2$. The converted ages were calculated using the following constants: $^{40}K/K = 1.167\ 10^{-4}$ g/g; $\lambda_\varepsilon = 0.572\ 10^{-10}$/a; $\lambda'_\varepsilon = 0.0088\ 10^{-10}$/a; $\lambda_\beta = 4.962\ 10^{-10}$/a. The error margin for the age is 2σ (Appendix Table A1).

https://doi.org/10.1017/S001675680800544X Published online by Cambridge University Press

Table 1. Major and trace element data for the cinder cones in the study area and the syenite from Montaña Pelada

Wt %	TF-4	TF-7.1	TF-8.1	TF-8.2	TF-9	TF-11	TF-12	TF-17	TF-18	TF-20	TF-21	TF-22	TF-23	TF-24	TF-30	TF-47	TF-P1
SiO_2	42.84	44.28	47.14	47.33	44.27	49.78	43.44	46.62	41.48	41.38	42.05	42.86	43.54	40.34	41.58	40.37	50.41
Al_2O_3	15.1	15.49	16.56	16.6	15.52	16.38	14.94	16.15	12.08	13.75	14.8	15.07	15.37	13.06	12.89	13.38	20.07
MnO	0.21	0.21	0.2	0.19	0.21	0.22	0.21	0.19	0.18	0.19	0.2	0.21	0.21	0.19	0.19	0.2	0.16
MgO	5.57	4.71	4.37	4.52	4.65	3.04	5.62	3.92	8.65	5.74	5.83	5.36	4.62	7.53	8.94	7.58	1.25
CaO	9.49	9.18	8.48	8.76	9.04	6.81	9.7	8.33	12.16	11.25	9.86	9.47	9.34	12.28	12.13	11.47	4.43
Na_2O	3.79	3.73	4.25	4.24	3.83	4.62	3.25	4.8	2.07	3.97	3.2	3.42	3.39	2.78	3.06	2.65	7.18
K_2O	1.7	1.78	1.97	1.89	1.83	2.21	1.59	2.35	1.11	2.04	1.57	1.76	1.9	1.6	1.45	1.35	3.2
TiO_2	3.3	3.36	3.1	3.13	3.4	2.03	3.89	2.94	3.24	4.3	4.11	4.05	3.55	4.1	3.81	3.76	1.28
P_2O_5	0.95	0.99	0.96	1.02	0.96	1.08	0.81	0.78	0.63	1.06	0.98	0.98	1.17	0.95	1.23	1.18	0.4
Fe_2O_3	11.97	12.2	11.87	11.75	12.33	9.05	12.96	9.68	12.66	12.5	13.25	13.28	12.47	13.62	14.12	13.07	5.37
ppm																	
V	167.22	171.88	195	190	188.99	62.23	251.94	187.13	270.12	308.21	249.66	238	208.47	315.93	321	257.42	24.4
Cr	70.68	25.98	18	18	3.7	3.15	19.14	10.84	447.56	69	2.23	0.89		158.57	268	138.15	4.6
Co	38.51	46.77	27	25	49.62	19.83	64.85	58.89	56.08	61.51	45	52.72	83.76	90.87	50	51.8	26.07
Ni			8	7			1.28	1.71	163.35	21.81				71.27	92	61.77	
Cu									37.38					30.56			
Zn	112.66	115.39	124	122	121.95	111.39	117.77	109.48	96.75	112.67	108.37	110.26	121.73	112.11	116	104.84	83.04
Ga	20.14	21.25	20	21	21.38	19.21	20.32	20.94	17.35	21.59	20.12	20.25	21.26	19.83	18	18.57	25.41
Ge	0.09						0.53	0.73	0.19	0.17		0.16	1.1	0.07		0.27	1.05
As	1	1.57				1.53	0.79	2.77	3.31	4.65			1.48	0.4		3.17	
Se		0.26				0.48	0.22	0.01	1.57	0.42						0.58	0.72
Br	14.95	0.92			1.12	0.48	0.99	1.47	0.71	1.58	0.9	0.01	0.85	0.95		3.14	1.27
Rb	40.61	42.61	43	40	44.09	36.42	34.15	52.74	19.42	43.29	31.77	34.06	37.57	36.05	24	27.27	70.23
Sr	1035.94	976.7	992	1006	990.63	1369.24	925.2	986.61	782.98	1158.97	976.41	978.04	1064.3	1018.22	1124	1016.55	1674.48
Y	30.85	31.95	38	35	32.49	35.27	31.69	32.77	23.88	33.27	31.26	31.81	33.77	29.61	36	29.36	30.24
Zr	382	395.8	454	439	400.95	493.54	360.67	423.95	243.34	350.35	329.44	345.48	378.75	325.02	282	272.95	540.31
Nb	99.64	101.74	109	108	104.06	94.41	79.01	121.16	61.95	99.25	75.73	77.59	86.35	90.74	77	71.05	164.02
Mo	2.87	2.97			2.5	2.06	2.33	3.28	0.44	2.99	1.87	1.92	2.2	2.24		1.93	3.09
Ag		3.77			1.35	0.25			3.05	1.33		0.74				0.04	
Cd		0.33							0.02								
Sn	1.36	1.06			1.31	1.11		1.74	0.08	1	0.49		1.31	0.56			0.6
Sb					0.52			0.43	0.48	0.15							0.06
Te																	
I	0.55										2.23						
Cs																	0.92
Ba	481.5	521.3	554	571	535.2	981.9	546.6	872.7	360.26	621.1	462	476.7	519.4	540.4	526	431.2	481.55
La	61.42	78.06	32	40	84.58	97.35	72.4	101.31	43.81	72.01	56.26	54.16	69.94	58.42	34	65.45	94.23
Ce	152.27	160.72	147	148	154.93	193.21	129.2	175.53	94.89	172.7	129.09	125.93	160.25	150.27	121	114.16	185.05
Pr	13.05	15.42	22	21	13.16	19.86	10.78	16.2	5.04	16.6	10.9	13.57	10.24	12.61	29	5.82	19
Nd	63.15	65.55			66.95	87.08	58.03	67.48	43.35	74.5	62.99	66.07	70.62	69.04		60.94	56.65
Sm	15.49	8.54			6.89	10.29	14.92	7.79	6.31	18.76	7.17	8.21	13.91	12.06		15.54	10.33
Yb	5.5	4.27				4.13	4.99	4.45	1.93	1.71				2.73		3.72	2.31
Hf	9.9	7.4			7.53	9.53	8.36	7.66	6.63	7.66	5.95	6.84	5.44	4.91		3.23	11.72
Ta	5.03	6.82			6.53	7.22	4.6	9.62	3.93	3.79	5.55	6.53	5.02	6.48		5.13	8.24
W	90.6	143.33			168.57	61.63	193.58	234.2	47.77	193.85	120.79	153.43	356.48	325.87		89.85	127.79
Tl		0.18															
Pb			5	4				0.38	0.45						4		0.37
Bi	0.82	1.47			0.78	1.25	0.65	1.12	2.89	1.76	1.8	1.11	1.67	2.29		2.21	0.43
Th	11.09	9.75	12	16	9.37	9.25	6.64	9.3	6.42	10.37	5.84	5.62	7.84	8.26	4	6.27	16.67
U	5.13	4.85			3.9	3.93	3.08	4.9	2.33	5.44	4.35	5.74	5.31	3.35		2.58	16.62

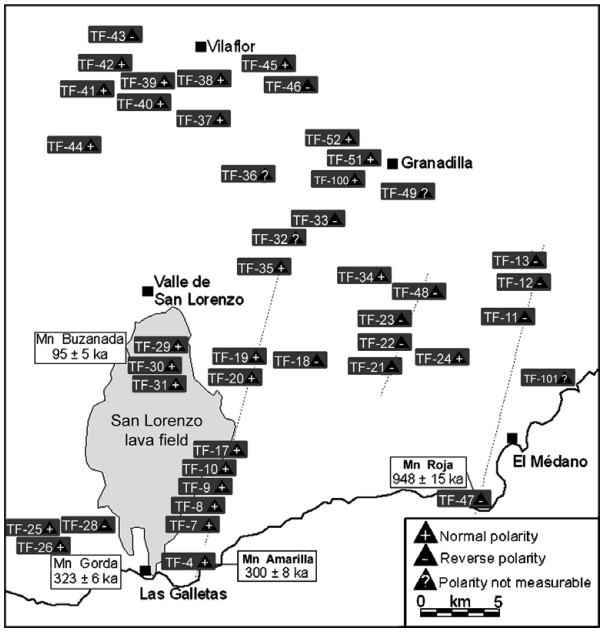

Figure 2. Position and magnetization of cinder cones in the study area. Light type: known K–Ar ages are given from Carracedo *et al.* (2007); bold type: new K–Ar ages presented in this study.

3. New data

3.a. Palaeomagnetic data

The cinder cones in the study area show both normal and reverse remanent magnetization (Fig. 2, Table 2, and Appendix Table A2). Thirteen cinder cones exhibit reverse polarities, 27 normal polarities, and four cinder cones do not show any clear palaeomagnetic signal (Fig. 2), due to either the lack of adequate volcanic bombs or to demagnetization induced by lightning (Graham, 1961). The locations (UTM-Coordinates) and sample denominations are listed in Table 2. According to the geomagnetic polarity time scale (GPTS), the last geomagnetic polarity reversal event (Matuyama/Brunhes) was dated at 778.7 ± 1.9 ka ago (Singer & Pringle, 1996). Accordingly, at least 13 cinder cones in the study area must be considered to be older than 778.7 ka (Figs 2, 3a–d). The other cones, displaying normal polarity, erupted during the Brunhes (> 778.7 ka).

3.b. Geochemical data

The geochemical data, in particular the immobile trace elements, were used as an additional tool to distinguish between the R-Basalts, N-Basalts and N-Basalts-SL. The results of the analyses for major and trace elements are presented in Table 1. Geochemically, the samples show an alkalic trend, plotting in the basanite, tephrite and trachybasalt field of the Total Alkali–Silica diagram (Le Bas *et al.* 1986). One sample plots in the field for basaltic trachyandesites (Fig. 4a). The SiO_2 contents range from 41.7 wt % to 47.5 wt % for N-Basalts and from 42.4 wt % to 52.1 wt % for R-Basalts, indicating that during the eruption of the N- and R-Basalts, the magma evolved from a primitive basanitic to a more differentiated melt (Fig. 4a).

Multi-element plots for several trace elements (Fig. 4b), normalized to primary mantle composition (Sun, 1980; McDonough *et al.* 1992), show enrichment in elements ranging from Rb to Ti as compared to N-MORB element distribution (Saunders & Tarney, 1984; Sun, 1980). Potassium is depleted relative to Ba, Th and Nb. The R- and N-Basalts and N-Basalts-SL exhibit chemical signatures typical for ocean island basalts and Canary Island basalts enriched in the more

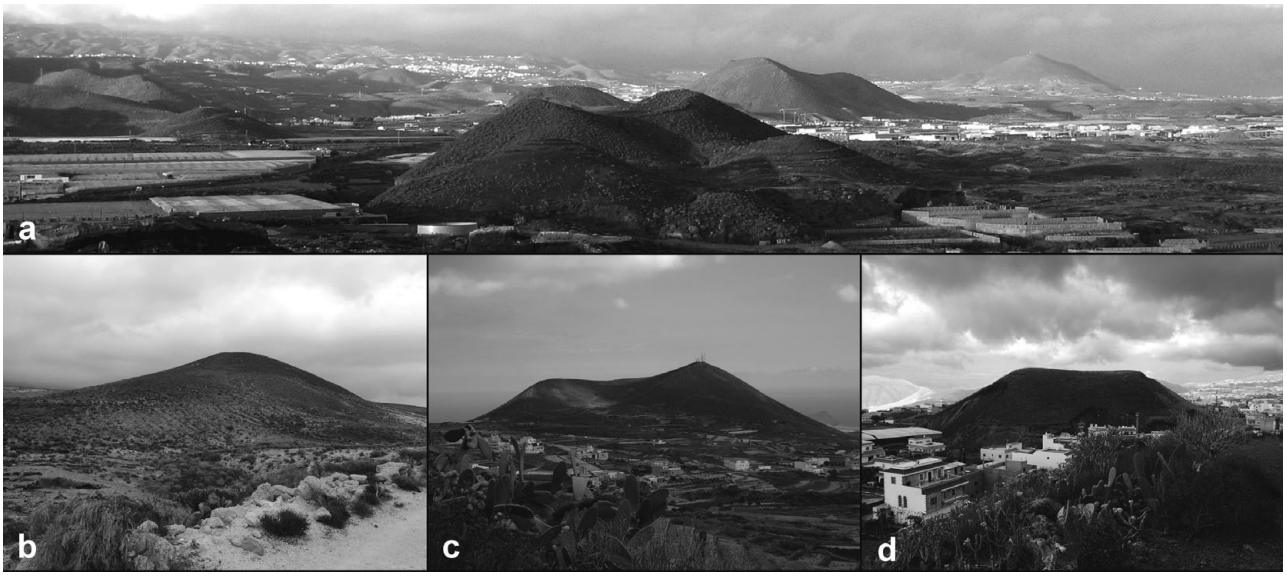

Figure 3. (a) General overview of the distribution of cinder cones within the Bandas del Sur, southern Tenerife; a chain of cinder cones orientated along the trend of the S-Rift can be recognized in the centre of the photo. (b) Intensively eroded cinder cone of Montaña Ifaro with gently inclined flanks that are partly covered by ignimbrites (constructional age of *c.* 950 ka, Cycle 2). (c) Slightly eroded cinder cone of Montaña Gorda with steep flanks (constructional age of *c.* 300 ka, Cycle 3). (d) Largely unweathered cinder cone of Buzanada with steep flanks and fresh scoria (constructional age of *c.* 100 ka, Cycle 4).

https://doi.org/10.1017/S001675680800544X Published online by Cambridge University Press

Table 2. UTM-coordinates, magnetization and trace element ratios for the cinder cones in the study area; XRF data are recalculated to anhydrous conditions

Sample	UTM-coordinates (WGS84)	Polarity	Y/Nb	Zr/Nb
TF-4/Amarilla	3099631N/28339167E	N	0.31	3.83
TF-7.1/Malpasito1	3100424N/28339243E	N	0.31	3.89
TF-7.2/Malpasito2	3100930N/28339122E	N		
TF-8.1/Chargo	3101784N/28339781E	N	0.35	4.17
TF-8.2/Chargo	3101848N/28339746E	N	0.32	4.06
TF-9/Negra	3101323N/28339139E	N	0.31	3.85
TF-10/Majano	3101965N/28339564E	N		
TF-11/Callao	3107521N/28349389E	R	0.37	5.23
TF-12/Ifaro	3108275N/28349783E	R	0.40	4.56
TF-13/NN	3108853N/28349792E	R		
TF-17/Erales	3103005N/28339988E	N	0.27	3.50
TF-18/Chimbesque	3105512N/28341186E	R	0.39	3.93
TF-19/Lucena	3105895N/28341054E	N		
TF-20/Estrella	3105291N/28340923E	N	0.34	3.53
TF-21/Casablanca	3105832N/28345242E	R	0.41	4.35
TF-22/Montanita	3106482N/28345360E	R	0.41	4.45
TF-23/Tabaibas	3106695N/28345314E	R	0.39	4.39
TF-24/Conde	3105889N/28345834E	N	0.33	3.58
TF-25/NN	3100703N/28333485E	N		
TF-26/GordaGrande	3100131N/28333752E	N		
TF-28/Laguneta	3100490N/28334116E	R		
TF-29/Cambada	3106140N/28338455E	N		
TF-30/Buzanada	3105855N/28338316E	N	0.47	3.66
TF-31/NN	3105609N/28337416E	N		
TF-32/VinaVieja	3104627N/28342152E	?		
TF-33/Chinama	3109934N/28343101E	R		
TF-34/Gorda	3108543N/28344013E	N		
TF-35/Garanana	3108762N/28341601E	N		
TF-36/Tileta	3111472N/28340945E	?		
TF-37/Pozo	3113370N/28339108E	N		
TF-38/Coto	3115207N/28338612E	N		
TF-39/DonaCandida	3114317N/28337397E	N		
TF-40/NN	3114554N/28337076E	N		
TF-41/Listones	3114666N/28336272E	N		
TF-42/Pinos	3115154N/28336571E	N		
TF-43/Vica	3116005N/28336960E	R		
TF-44/Funes	3112318N/28336055E	N		
TF-45/Mesas	3115013N/28340697E	N		
TF-46/Coloradas	3114371N/28341470E	R		
TF-47/Roja	3101247N/28348249E	R	0.41	3.84
TF-48/Yaco	3107799N/28346504E	R		
TF-49/Acojea	3111293N/28345288E	?		
TF-51/Chozas	3111752N/28343973E	N		
TF-52/Tea	3112486N/28343864E	N		
TF-100/NN	3108473N/28342523E	N		
TF-101/Pelada	3104740N/28350552E	?		

N: normal polarity; R: reverse polarity.

incompatible elements and a negative K anomaly (Ancochea & Huertas, 2003), similar to those of HIMU-type basalts (Weaver 1991). The N-, R-Basalts and N-Basalts-SL show comparable chemical signatures, indicating that they all were derived from the same mantle source (Fig. 4b). The content of lithophile elements like Na_2O, K_2O, Rb and Nb increases with decreasing MgO content (Fig. 5). The depletion of CaO, Fe_2O_3 and V with decreasing MgO is indicative of fractionation processes involving the formation of olivine, titanoferous magnetite and clinopyroxene (Price & Chappell, 1975). The N-Basalts are generally more enriched in Na_2O, K_2O and in the incompatible elements at similar MgO concentrations compared to the R-Basalts and N-Basalts-SL (Fig. 5). This may indicate that the N-Basalts were generated as a result of lower degrees of partial melting. The trace element plot Y/Nb versus Zr/Nb separates the R-Basalts, the N-Basalts and the N-Basalts-SL into three well-defined fields (Fig. 6). The N-Basalts exhibit Y/Nb ratios < 0.35, the R-Basalts show Y/Nb ratios between 0.37 and 0.41 and the N-Basalts-SL display Y/Nb ratios ~ 0.47 (Table 2). Additionally, this plot is useful to evaluate the degree of enrichment of the mantle source (Pearce & Norry, 1979; Abratis, Schmincke & Hansteen, 2002); hence, the N-Basalts are derived from a more enriched mantle source compared to R-Basalts and N-Basalts-SL (see Fig. 6).

3.c. K–Ar age determination

Age determination resulted in an age of 300 ± 8 ka for the sample TF-4/Amarilla (N-Basalts) and 948 ± 15 ka for the sample TF-47/Roja (R-Basalts) (Table 2). Carracedo *et al.* (2003, 2007) presented K–Ar ages of 95 ± 5 ka for a cinder cone near La Buzanada, 323 ± 6 ka for the cinder cone Montaña Gorda, and 311 ± 6 ka for a basaltic lava flow at the Autopista Sur km 30. The cinder cone near La Buzanada comprises N-Basalts-SL, while Montaña Gorda comprises N-Basalts

https://doi.org/10.1017/S001675680800544X Published online by Cambridge University Press

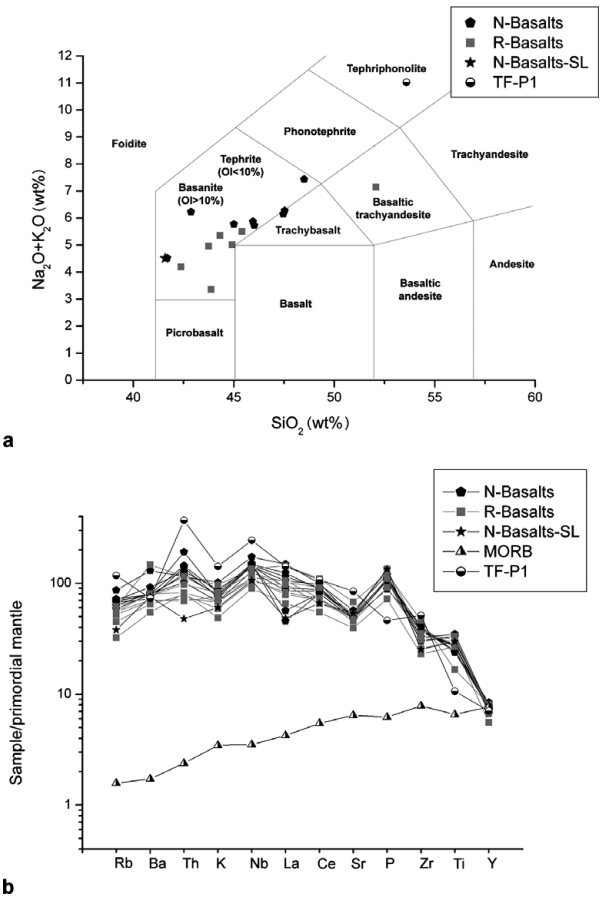

Figure 4. (a) Classification of the R-Basalts (reverse polarity), N-Basalts (normal polarity), N-Basalts-SL (normal polarity, San Lorenzo lava field) and syenite (tephriphonolite; TF-P1) using the TAS-diagram (Le Bas *et al.* 1986). (b) Multi-element plot for the R-Basalts, N-Basalts and the syenite (tephriphonolite), normalized to primordial mantle (Sun, 1980; McDonough *et al.* 1992). The MORB-line is taken from Saunders & Tarney (1984) and Sun (1980).

(Fig. 2, Table 2). Based on these dates, a minimum age for the R-Basalts is between the last geomagnetic polarity reversal event (Matuyama/Brunhes) at 778.7 ± 1.9 ka (Singer & Pringle, 1996) and the K–Ar age of 948 ± 15 ka (TF-47/Roja). The eruption of N-Basalts started at a minimum age between 323 ± 6 ka and 300 ± 8 ka. Volcanic activity of the San Lorenzo lava field began *c.* 95 ± 5 ka ago (Fig. 7).

4. Characteristics of the S-Rift

Compared to the NW- and NE-Rift, the evolution of the southern rift zone proceeded unequally in many respects. The NW- and NE-Rift zones display steep ridges built up by fissure eruptions and are characterized by a narrow chain of cinder cones and an extensional stress field, triggering flank collapses (e.g. Icod, Orotava, Güimar: Carracedo *et al.* 2007). Eruptive activity along the NE- and NW-Rift located in medial and distal zones of the Las Cañadas caldera mainly produced mafic lavas; felsic eruptions exclusively occurred in proximal zones near or within the caldera (Carracedo *et al.* 2007).

In the S-Rift the volcanic features are arranged in widely scattered clusters and parallel chains following the direction of the S-Rift (Fig. 2); it does not display a distinct ridge and instead has a fan-shaped distribution of the monogenetic cones (fig. 1 in Carracedo *et al.* 2007). In the distal part of the southern rift zone, basaltic cinder cones occur together with two phonolitic eruption centres (Montaña Guaza and Caldera del Rey). According to Martí, Andujar & Wolff (2004), the phonolitic centres (see Figs 1, 8a) represent the only manifestations of highly evolved magma outside the Las Cañadas caldera. In the tuff cone deposits of Montaña Pelada, syenitic components ('tephriphonolite' TF-P1 in Fig. 4a, b) occur as ballistic blocks ranging from a few centimetres to about 1 m in size (Fig. 8b). The syenitic components of intermediate character (Fig. 4) are composed of K-feldspar, plagioclase and feldspathoides (mainly nepheline) (Fig. 8c). On Tenerife, syenitic rock fragments have been described exclusively as components of ignimbrites (e.g. El Abrigo ignimbrite: Wolff, Grandy & Larson, 2000) that were derived from the Las Cañadas edifice; the tuff cone deposits of Montaña Pelada, however, do not display any components derived from reworked ignimbrites. Wolff (1987) proposed that the Tenerife syenitic components crystallized on the roof of a phonolitic magma chamber.

5. Discussion

5.a. S-Rift zone

According to Walter & Troll (2003), the triaxial architecture of the rift zones on Tenerife is characteristic of a volcano that is centrally supplied with magma and is experiencing increases in the instability of a sector. This results in two rift zones with intense volcanic activity (corresponding with the NW- and NE-Rift zone on Tenerife) and a less pronounced rift zone, located in the stable part of the volcano (corresponding with the S-Rift zone on Tenerife). Acosta *et al.* (2003) described rift characteristics of the nearby islands of La Palma and El Hierro that are comparable to the S-Rift of Tenerife. These are characterized by a broad fan-like distribution of monogenetic centres. They relate this to the stress field within the rift being insufficient to trap dykes within a narrow region and/or to dyke injection and volcanism shifting laterally through time. Additionally, a low rate of magma supply produces low magma pressures, responsible for randomly orientated dyke injections. The rift zones of the Hawaiian Islands generally consist of linear and steep ridges. The toes of some Hawaiian rifts partly fan out as well, perhaps as a result of low magma supply (Acosta *et al.* 2003).

In the distal part of the S-rift zone, basaltic cinder cones are associated with volcanic features formed by phonolitic eruptions (Fig. 9a, b). Additionally, syenitic components (TF-P1, Fig. 4) occur as ballistic blocks

https://doi.org/10.1017/S001675680800544X Published online by Cambridge University Press

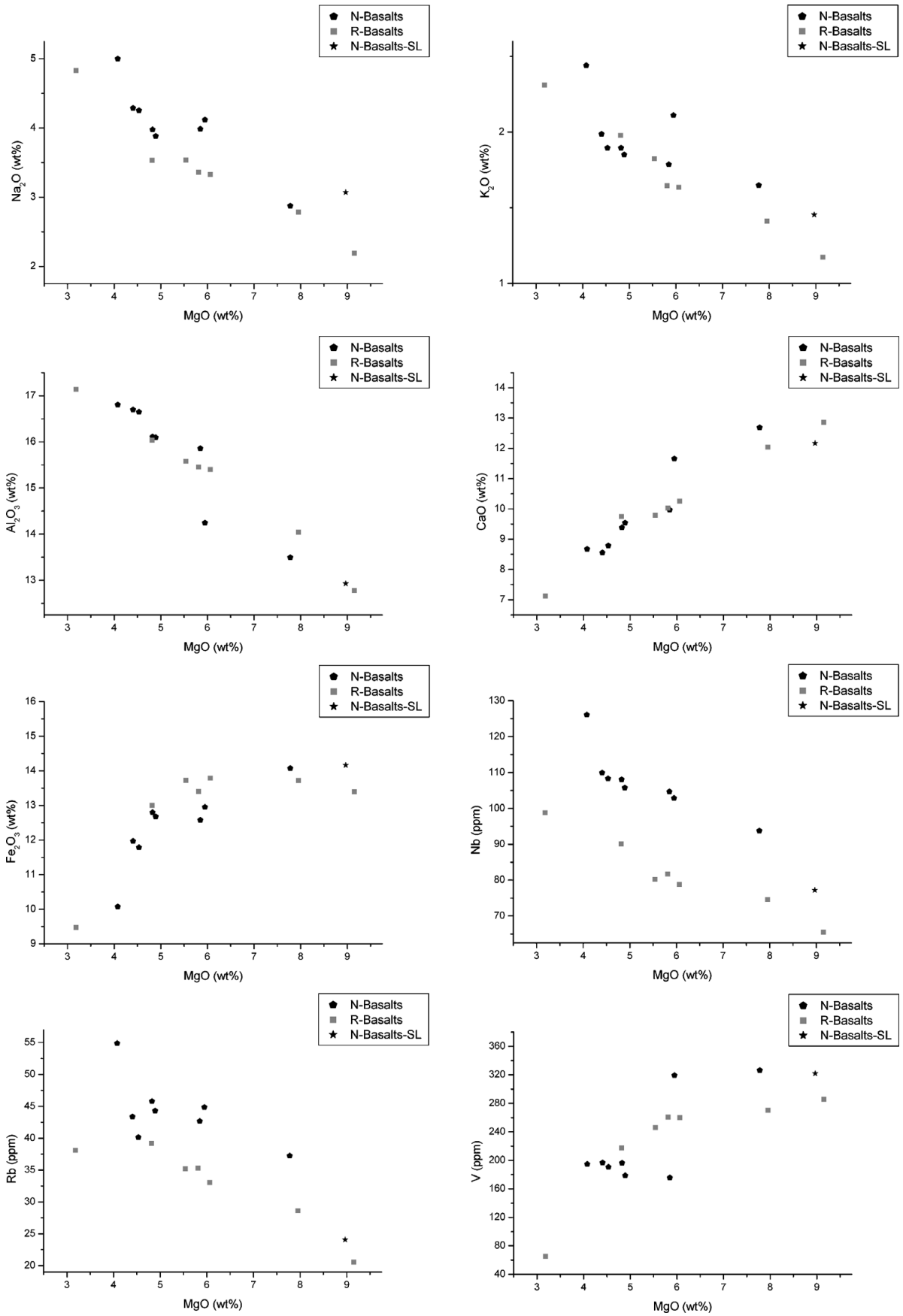

Figure 5. Incompatible and compatible elements plotted against MgO for the samples studied in this work.

https://doi.org/10.1017/S001675680800544X Published online by Cambridge University Press

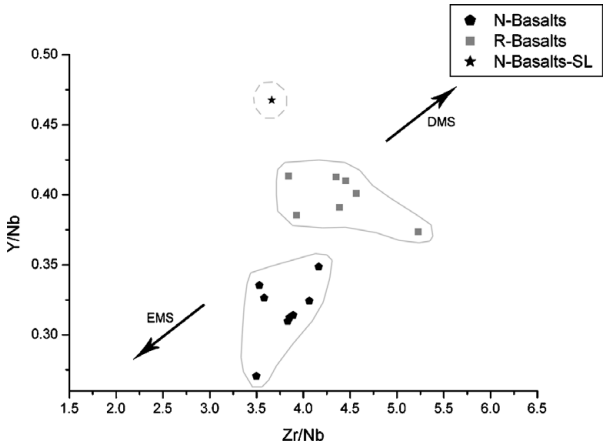

Figure 6. Trace element variations between the R-Basalts, N-Basalts and N-Basalts-SL showing different mantle source characteristics; modified after Pearce & Norry (1979). EMS – enriched mantle source; DMS – depleted mantle source.

in the tuff cone of Montaña Pelada. Widom, Gill & Schmincke (1993) interpreted syenitic ballistic blocks at the Agua de Pao Volcano on the island of San Miguel (Azores) as fragments that had crystallized in the margins of a magma chamber ejected during an explosive eruption. Together with the phonolitic volcanic centres of Montaña Guaza and Caldera del Rey, we interpret the occurrence of syenitic rocks as evidence for shallow magma pockets, located in the distal part of the S-Rift (compare to Fig. 9b).

5.b. Cyclicity of volcanic activity

The major pyroclastic deposits in the Bandas del Sur correlate with eruptions that built up the major ignimbrite layers of the Ucanca, Guajara and Diego Hernández Formation cropping out in the caldera wall. According to Martí, Mitjavila & Araña (1994) and Bryan, Martí & Cas (1998), these formations represent three volcanic cycles: each cycle started with mafic flank eruptions and culminated in an explosive, caldera-forming eruption, collectively responsible for the development of the Las Cañadas caldera (Martí *et al.* 1997). According to Brown *et al.* (2003) and Edgar *et al.* (2007), numerous ignimbrite layers and pumice fall deposits of the Bandas del Sur give evidence for more than three caldera collapse events and a more complex development of the Las Cañadas caldera. On the other hand, the three cycles, represented by major pyroclastic deposits within the Bandas del Sur, are separated from each other by longer periods without significant volcanic activity, erosional disconformities and palaeosoils which are discordantly overlain by basaltic lava flows. In the aftermath of periods of non-pyroclastic deposition, ascending magma in the Las Cañadas volcano probably has been responsible for increasing flank eruptive activity in the southern rift zone, producing large lava fields and cinder cones.

Volcanic eruption cycles for the Santorini volcano (Greece) with an average duration of about 180 ka

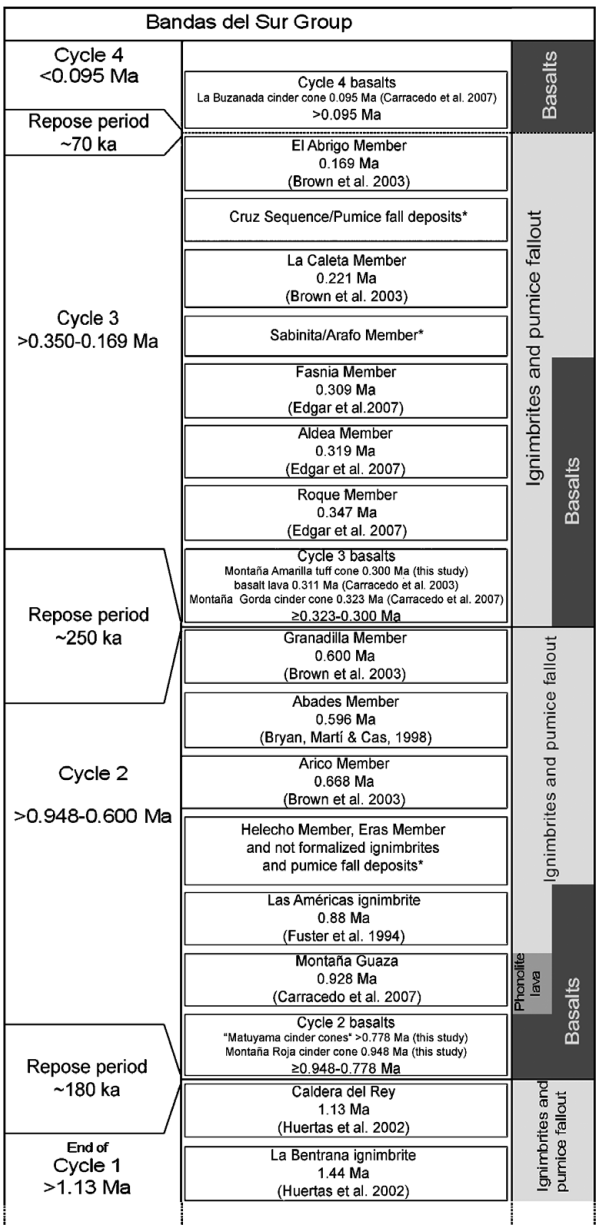

Figure 7. Volcanic cycles documented in the Bandas del Sur and related volcanic deposits. Data sources: Fuster *et al.* (1994); Bryan, Martí & Cas (1998); Bryan, Martí & Leosson (2002); Huertas *et al.* (2002); Brown *et al.* (2003); Carracedo *et al.* (2003, 2007) and Edgar *et al.* (2007). For volcanic deposits that are not absolutely dated, the relative age is defined by their stratigraphic position.

have been described by Druitt *et al.* (1989), Druitt *et al.* (1999) and Zellmer, Turner & Hawkesworth (2000); each cycle ended with a major caldera-forming eruption. According to Christiansen (2001), the volcanic activity of the Yellowstone caldera volcano (Wyoming, USA) is characterized by three volcanic cycles during the last 2.1 Ma; each cycle totals about 640 ka to 800 ka. The early stage has been dominated by plateau basalt eruptions and each cycle ended with a major caldera forming eruption. However, basaltic as well as rhyolitic eruptions accompanied the entire period of volcanic activity. The time span of major volcanic activity of the three cycles ranges from about

https://doi.org/10.1017/S001675680800544X Published online by Cambridge University Press

Figure 8. (a) View northward to the phonolitic dome and flow complex of Montaña Guaza; phonolitic lava flow (behind the housing) is tens of metres thick; the phonolitic lava dome of Montaña Guaza is situated centre-right of the photograph. (b) Syenitic (tephriphonolitic) nodule as ballistic block in the tuff cone deposits of Montaña Pelada east of El Médano. (c) Thin-section micrograph of the syenitic component (Montaña Pelada) showing hypidiomorphic K-feldspar and plagioclase crystals.

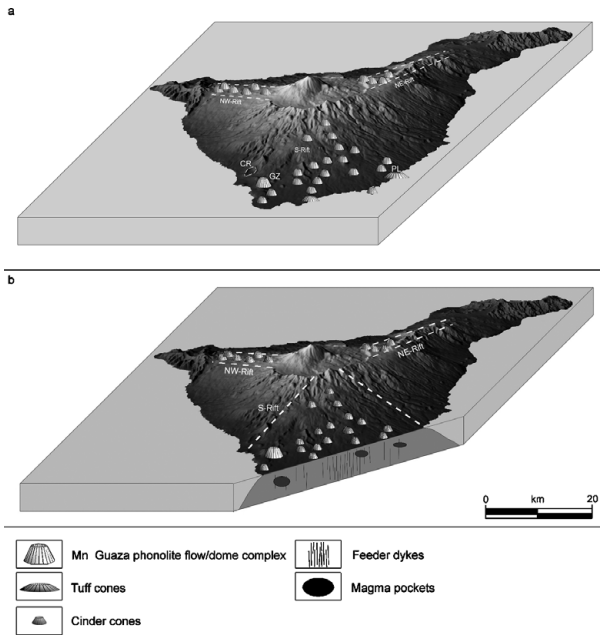

Figure 9. (a) Model of the triaxial rift zone on Tenerife illustrating the distribution of cinder cones; narrow chains of cinder cones on top of the steep ridges of the NW- and NE-Rift and a fan-like distribution of monogenetic volcanic structures within the S-Rift. (b) Interpretation of the occurrence of phonolitic volcanic structures in the distal part of the S-Rift with feeder dykes and assumed magma pockets underneath the Bandas del Sur. CR – Caldera del Rey; GZ – Montaña Guaza; PL – Montaña Pelada.

340 ka to 580 ka, and the repose periods between the cycles from about 140 ka to 520 ka, respectively (Christiansen, 2001).

5.c. Stratigraphy

Based on the dataset presented in this work and on the radiometric age dating of several volcanic units in previous literature, we define four volcanic cycles based on the stratigraphy developed by Bryan, Martí & Cas (1998), Brown *et al.* (2003) and Edgar *et al.* (2007) for the Bandas del Sur (Fig. 7). The volcanic cycles 1 to 4 depicted in Figure 7 are defined for the volcanic succession of the Bandas del Sur Group; in the NW- and NE-Rift, due to the lack of ignimbrites, a volcanic cyclicity has not yet been identified. According to Galindo & Soriano (2005), fissure eruptions along the NE-Rift have occurred since the early development of the rift up to the historical eruptions. Cycle 1 deposits are scarce in the Bandas del Sur and Cycle 1 is poorly defined in age and distribution. Pyroclastic deposits of Cycle 1 are preserved in the southwestern flank of Tenerife; however, the stratigraphic position of these units is not well defined. Additionally, neither the Helecho Member nor the Arafo Member of the Bandas del Sur Group have been dated yet. Further dating of pyroclastic deposits and lavas is necessary to constrain better the duration of each cycle. Cinder

https://doi.org/10.1017/S001675680800544X Published online by Cambridge University Press

cones belonging to Cycle 1 have not yet been found in the study area.

The alignments of Cycle 2, 3 and 4 cinder cones occur mainly along NNE–SSW trends (Fig. 2), representing the main direction of the S-Rift zone (Figs 1a, 8a). The specific alignment indicates that persistent fractures acted as continuous channels for the mafic flank eruptions within the Bandas del Sur (Bryan, Martí & Cas, 1998; Bryan, Martí & Leosson, 2002). In previous literature, all the cinder cones within the study area (except the San Lorenzo cinder cones) were assigned to the Cycle 3/Series III-basalts (e.g. Fuster *et al.* 1968; Bryan, Martí & Cas, 1998; Bryan, Martí & Leosson, 2002; Clarke *et al.* 2005) with an eruption age between 690 ka and the Upper Pleistocene/Holocene boundary (e.g. Bellido Mulas *et al.* 1978; Hernández-Pacheco & Fernández Santín, 1978; Carracedo, 1979) or > 320–316 ka (Bryan, Martí & Cas, 1998).

The palaeomagnetic data and K–Ar ages determined through this study indicate that a specific number of cinder cones belong to an older volcanic cycle. At least 13 cinder cones show reverse magnetization (R-Basalts; Fig. 2) and hence they must be older than the last geomagnetic polarity reversal event at 778.7 ± 1.9 ka (Singer & Pringle, 1996). The cones represent the initial stage of Cycle 2 eruptions. Bryan, Martí & Cas (1998) set the beginning of Cycle 2 to a minimum age of > 760 ka. Using the age of TF-47/Roja (948 ± 15 ka) and the palaeomagnetic data, the start of flank eruptive activity at the base of Cycle 2 can be set at between $> 948 \pm 15$ ka and 778.7 ± 1.9 ka (Fig. 7).

The basalts showing normal magnetization (N-Basalts and N-Basalts-SL; Fig. 2) belong to Cycle 3 and to the San Lorenzo lava field. The assumed onset of Cycle 3 > 320 ka ago (Bryan, Martí & Cas, 1998) correlates with the age of the cinder cone Montaña Gorda and with a lava flow by Carracedo *et al.* (2003, 2007), as well as with the age of TF-4/Amarilla, presented in this study. It can be assumed that the majority of basaltic flank eruptions at the base of Cycle 3 took place between 323 ± 6 ka and 300 ± 8 ka.

The basaltic eruptions of the San Lorenzo lava field indicate the start of a possible further volcanic cycle (Kröchert, Maurer & Buchner, 2008). The age of the San Lorenzo lava field is given from the K–Ar age of a cinder cone near La Buzanada (Carracedo *et al.* 2007), defining the onset of Cycle 4 to a minimum age of > 95 ka. The caldera-forming eruptions of Cycle 3 have been followed by the construction of the Pico de Teide and Pico Viejo stratocones that began with non- or minor-explosive eruptions of basaltic to intermediate and phonolitic lavas inside the Las Cañadas caldera; basaltic fissure eruptions occurred concurrently along the NW- and NE-Rift (Carracedo *et al.* 2007). The subplinian eruption of Montaña Blanca (Fig. 1) about 2 ka ago (Ablay *et al.* 1995) may represent a change from effusive basaltic flank eruptions and non-explosive volcanism at Pico de Teide and Pico Viejo to a more explosive phase (Bryan, Martí & Cas, 1998; Wolff, Grandy & Larson, 2000), similar to the earlier volcanic cycles (Fig. 7).

The ends of the four cycles defined in this study are characterized by widespread erosional unconformities in the Bandas del Sur, by thick palaeosoil development (Bryan, Martí & Cas, 1998) and by extended periods without explosive volcanic eruptions. The gap between Cycles 1 and 2 lasted for about 180 ka, between Cycles 2 and 3 for about 250 ka, and between 3 and 4 for about 70 ka. The period of volcanic activity of Cycle 2 lasted for about 350 ka and of Cycle 3 for 180 ka (compare with Fig. 7).

5.d. Geochemistry

The geochemical data reveal a magmatic evolution from primitive magma (SiO_2 41.7 wt %) to a more evolved tephritic and trachybasaltic magma for the R-Basalts and N-Basalts, due to fractional crystallization processes involving the removal of olivine, clinopyroxene and titaniferous magnetite (Figs 4, 5). The N-Basalts-SL, with high MgO, Fe_2O_3, V and Cr abundances represent a primitive magma with relatively short storage periods. Rapid ascent of magma from the mantle to upper crustal levels was proposed by Neumann, Wulff-Pedersen & Simonsen (1999), based on the presence of ultramafic xenoliths in the cinder cones and dykes of Tenerife. The range in the trace element abundances of the R-Basalts and N-Basalts (Fig. 4) could be explained by fractional crystallization processes, assimilation or different degrees of partial melting of the mantle source. Lower alkali (Na_2O+K_2O), Rb and Nb contents of the R-Basalts at similar MgO content in comparison to the N-Basalts and N-Basalts-SL (Fig. 5) may suggest a higher degree of partial melting. Immobile trace element plots for Y/Nb versus Zr/Nb (Pearce & Norry, 1979) show that the basalts plot into three different fields. The N-Basalts with Y/Nb ratios < 0.35 indicate that they were derived from a more enriched mantle source compared to the R-Basalts (Y/Nb: 0.37–0.41) and the N-Basalts-SL (Y/Nb: ~ 0.47); however, these ratios could also be influenced by magma mixing and mingling processes, characteristic for magma compositions on Tenerife (Ablay *et al.* 1998; Bryan, Martí & Leosson, 2002; Bryan, 2006). Fractional crystallization in periodically refilled magma chambers and the assimilation of syenite and amphibolite are also processes, present on Tenerife, which can change element ratios/abundances (Neumann, Wulff-Pedersen & Simonsen, 1999; Simonsen, Neumann & Seim, 2000) and may overprint primary mantle source characteristics. However, the Y/Nb versus Zr/Nb plot combined with the palaeomagnetic data appears to be a good tool to determine the stratigraphic position of cinder cones within the Bandas del Sur.

6. Conclusions

(1) The S-Rift zone has characteristics (morphological features, geochemistry of the volcanic deposits)

https://doi.org/10.1017/S001675680800544X Published online by Cambridge University Press

that are different from those of the NW- and NE-Rift zones. It does not display a distinct ridge and has a fan-shaped distribution of monogenetic cones. Together with phonolitic volcanic structures, we interpret the occurrence of syenitic rocks as evidence for shallow magma pockets, located in the distal part of the S-Rift.

(2) We identified four volcanic cycles in the volcanic succession of the Bandas del Sur; cycles 1 to 3 commenced with intense mafic flank eruptions and culminated in a series of explosive phonolitic eruptions. However, the formation of phonolitic volcanic structures outside the caldera as well as caldera forming eruptions occurred over a longer period and are not necessarily restricted to the final stage of each cycle.

(3) We define the end of each cycle by the occurrence of erosional unconformities, palaeosoils and longer periods without volcanic activity. The gap between Cycle 1 and 2 lasted for about 180 ka, between Cycle 2 and 3 for about 250 ka, and between 3 and 4 for about 70 ka.

(4) The cinder cones within the Bandas del Sur can be split into three different age groups, belonging to the Cycle 2, 3 and 4 episodes of basaltic flank volcanism.

(5) The Cycle 2 cinder cones have a wide distribution in the Bandas del Sur Formation and were erupted between $> 948 \pm 15$ ka and 778.7 ± 1.9 ka.

(6) The main eruptive activity of the Cycle 3 basalts occurred between 323 ± 6 ka and 300 ± 8 ka.

(7) The basaltic eruptions which formed the San Lorenzo lava field abut 95 ka ago may define the start of a fourth volcanic cycle.

Acknowledgements. We kindly thank Dr Steffen Kutterolf for helping us to improve the quality of our manuscript. We would also like to thank Dr Holger Maurer and Martin Schmieder for helpful comments and Anita Czambor for sample preparation and assistance during analytical work. We are grateful to the following institutions for financial support: Stifterverband für die Deutsche Wissenschaft and Graduiertenförderung des Landes Baden-Württemberg. Our London colleague Hilary Randall, who proofread the manuscript, is kindly acknowledged. We are grateful to the two reviewers, Prof. Dr Juan Carlos Carracedo and Dr Richard James Brown, for detailed and helpful comments on our manuscript.

References

ABLAY, G. J., CARROL, M. R., PALMER, M. R., MARTÍ, J. & SPARKS, R. S. J. 1998. Basanite–phonolite lineages of Teide–Pico Viejo volcanic complex, Tenerife, Canary Islands. *Journal of Petrology* **39**, 905–36.

ABLAY, G. J., ERNST, G. G. J., MARTÍ, J. & SPARKS, R. S. J. 1995. The ~2 ka subplinian eruption of Montaña Blanca, Tenerife. *Bulletin of Volcanology* **57**, 337–55.

ABLAY, G. J. & MARTÍ, J. 2000. Stratigraphy, structure, and volcanic evolution of Pico Teide–Pico Viejo formation, Tenerife, Canary Islands. *Journal of Volcanology and Geothermal Research* **103**, 175–208.

ABRATIS, M., SCHMINCKE, H.-U. & HANSTEEN, T. H. 2002. Composition and evolution of submarine volcanic rocks from the central and western Canary Islands. *International Journal of Earth Science* **91**, 562–82.

ACOSTA, J., UCHUPI, E., SMITH, D., MUÑOZ, A., HERRANZ, P., PALOMO, C., LIANES, P., BALLESTEROS, M. & ZEE WORKING GROUP. 2003. Comparison of volcanic rifts on La Palma and El Hierro, Canary Islands and the Islands of Hawaii. *Marine Geophysical Researches* **24**, 59–90.

ANCOCHEA, E., FUSTER, J. M., IBARROLA, E., CENDERO, A., COELLO, J., HERNAN, F., CANTAGREL, J. M. & JAMOND, C. 1990. Volcanic evolution of the island of Tenerife (Canary Islands) in the light of new K–Ar data. *Journal of Volcanology and Geothermal Research* **44**, 231–49.

ANCOCHEA, E. & HUERTAS, M. J. 2003. Age and composition of the Amanay Seamount, Canary Islands. *Marine Geophysical Researches* **24**, 161–9.

ARAÑA, V., BARBERI, F. & FERRARA, G. 1989. El complejo volcánico del Teide–Pico Viejo. In *Los Volcanes y La Caldera del Parque Nacional del Teide (Tenerife, Islas Canarias)* (eds J. Callao & V. Araña), pp. 101–26. Madrid: ICONA.

BELLIDO MULAS, F., BRANDLE MATESANZ, J. L., HERNÁNDEZ-PACHECO, A. & FERNÁNDEZ SANTÍN, S. 1978. *Mapa geológico de España, 1:25000*. 1.118-II. Valle de San Lorenzo. IGME.

BROWN, R. J., BARRY, T. L., BRANNEY, M. J., PRINGLE, M. S. & BRYAN, S. E. 2003. The Quaternary pyroclastic succession of southeast Tenerife, Canary Islands: explosive eruptions, related caldera subsidence, and sector collapse. *Geological Magazine* **140**, 265–88.

BRYAN, S. E. 2006. Petrology and Geochemistry of the Quaternary Caldera-forming, Phonolitic Granadilla Eruption, Tenerife (Canary Islands). *Journal of Petrology* **17**, 1557–89.

BRYAN, S. E., MARTÍ, J. & CAS, R. A. F. 1998. Stratigraphy of the Bandas del Sur Formation: an extracaldera record of the Quaternary phonolitic explosive eruptions from the Las Cañadas edifice, Tenerife (Canary Islands). *Geological Magazine* **135**, 605–36.

BRYAN, S. E., MARTÍ, J. & LEOSSON, M. 2002. Petrology and Geochemistry of the Bandas del Sur Formation, Las Cañadas Edifice, Tenerife (Canary Islands). *Journal of Petrology* **43**, 1815–56.

CARRACEDO, J. C. 1979. *Paleomagnetismo e historia volcanica de Tenerife Aula de Cultura*. Cabildo Insular de Tenerife, Tenerife, 81 pp.

CARRACEDO, J. C. 1994. The Canary Islands: an example of structural control on the growth of large oceanic-island volcanoes. *Journal of Volcanology and Geothermal Research* **60**, 225–41.

CARRACEDO, J. C., PATERNE, M., GUILLOU, H., PÉREZ TORRADO, F. J. & PARIS, R. 2003. Dataciones radiometricas (14C Y K/Ar) del Teide y el rift nordoeste, Tenerife, Islas Canarias. *Estudios Geologicos* **59**, 15–29.

CARRACEDO, J. C., RODRÍGUEZ BADIOLA, E., GUILLOU, H., PATERNE, M., SCAILLET, S., PEREZ TORRADO, F. J., PARIS, R., FRA-PALEO, U. & HANSEN, A. 2007. Eruptive and structural history of Teide Volcano and rift zones on Tenerife, Canary Islands. *Geological Society of America Bulletin* **119**, 1027–51.

CHRISTIANSEN, R. L. 2001. *The Quaternary and Pliocene Yellowstone plateau volcanic field of Wyoming, Idaho, and Montana*. U.S. Geological Survey, Professional Paper 729-G, 145 pp. Reston, Virginia.

CLARKE, H., TROLL, V. R., CARRACEDO, J. C., BYRNE, K. & GOULD, R. 2005. Changing eruptive styles and textural features from phreatomagmatic to Strombolian activity of basaltic littoral cones: Los Erales cinder cone, Tenerife, Canary Islands. *Estudios Geologicos* **61**, 121–34.

DOELL, R. R. & COX, A. 1962. Determination of the magnetic polarity of rock samples in the field. *U.S. Geological Survey Research* **450-D**, 105–8.

DRUITT, T. H., EDWARDS, L., MELLORS, R. A., PYLE, D. M., SPARKS, R. S. J., LANPHERE, M., DAVIES, M. & BARREIRO, B. 1999. *Santorini volcano*. Geological Society of London, Memoir no. 19, 165 pp.

DRUITT, T. H., MELLORS, R. A., PYLE, D. M. & SPARKS, R. S. J. 1989. Explosive volcanism on Santorini, Greece. *Geological Magazine* **126**, 95–126.

EDGAR, C. J., WOLFF, J. A., OLIN, P. H., NICHOLS, H. J., PITTARI, A., CAS, R. A. F., REINERS, P. W., SPELL, T. L. & MARTÍ, J. 2007. The late Quaternary Diego Hernandez Formation, Tenerife: Volcanology of a complex cycle of voluminous explosive phonolitic eruptions. *Journal of Volcanology and Geothermal Research* **160**, 59–85.

FUSTER, J. M., ARAÑA, V., BRANDLE, J. L., NAVARRO, J. M., ALONSO, U. & APARICIO, A. 1968. *Geology and volcanology of the Canary Islands: Tenerife*. Madrid: Instituto Lucas Mallada, CSIC, 218 pp.

FUSTER, J. M., IBARROLA, E., SNELLING, N. J., CANTAGREL, J. M., HUERTAS, M. J., COELLO, J. & ANCOCHEA, E. 1994. Cronología K–Ar de la Formación Cañadas en el sector Suroeste de Tenerife: Implicaciones de los episodios piroclásticos en la evolución volcánica. *Boletin de la real Sociedad Española de Historia Natural (Seccion geologica)* **89**, 25–41.

GALINDO, I. & SORIANO, C. 2005. Structural evolution of the NE rift zone of Tenerife, Canary Islands. *Geophysical Research Abstracts* **7**, EGU05-A-05367.

GRAHAM, K. W. T. 1961. The remagnetization of a surface outcrop by lightning currents. *Geophysical Journal* **6**, 85–102.

GUILLOU, H., CARRACEDO, J. C., PARIS, R. & PÉRÈZ TORRADO, F. J. 2004*a*. Implications for early shield-stage evolution of Tenerife from K/Ar ages and magnetic stratigraphy. *Earth and Planetary Science Letters* **222**, 599–614.

GUILLOU, H., PEREZ TORRADO, F. J., HANSEN MACHIN, A. R., CARRACEDO, J. C. & GIMENO, D. 2004*b*. The Plio-Quaternary volcanic evolution of Gran Canaria based on new K–Ar ages and magnetostratigraphy. *Journal of Volcanology and Geothermal Research* **135**, 221–46.

HERNÁNDEZ-PACHECO, A. & FERNÁNDEZ SANTÍN, S. 1978. *Mapa geológico de España, 1:25000*. 1.119-IV. Lomo de Arico. IGME.

HUERTAS, M. J., ARNAUD, N. O., ANCOCHEA, E., CANTAGREL, J. M. & FÚSTER, J. M. 2002. $^{40}Ar/^{39}Ar$ stratigraphy of pyroclastic units from the Cañadas Volcanic Edifice (Tenerife, Canary Islands) and their bearing on the structural evolution. *Journal of Volcanology and Geothermal Research* **115**, 351–65.

KRÖCHERT, J., MAURER, H. & BUCHNER, E. 2008. Fossil beaches as evidence for significant uplift of Tenerife, Canary Islands. *Journal of African Earth Sciences* **51**, 220–34.

LE BAS, M. J., LE MAITRE, R. W., STRECKEISEN, A. & ZANETTIN, B. 1986. A Chemical Classification of Volcanic Rocks Based on Total Alkali–Silica Diagram. *Journal of Petrology* **27**, 745–50.

MARTÍ, J., ANDUJAR, J. & WOLFF, J. A. 2004. Interaction between basaltic and phonolitic magma systems in Tenerife (Canary Islands): Implications for eruptive dynamics. *Geophysical Research Abstracts* **6**, EGU04-A-04799.

MARTÍ, J., HURLIMANN, M., ABLAY, G. J. & GUDMUNDSSON, A. 1997. Vertical and lateral collapse on Tenerife (Canary Islands) and other volcanic ocean islands. *Geology* **25**, 879–82.

MARTÍ, J., MITJAVILA, J. & ARAÑA, V. 1994. Stratigraphy, structure and geochronology of the Las Cañadas caldera (Tenerife, Canary Islands). *Geological Magazine* **131**, 715–27.

MCDONOUGH, W. F., SUN, S., RINGWOOD, A. E., JAGOUTZ, E. & HOFMAN, A. W. 1992. K, Rb, and Cs in the earth and moon and the evolution of the earth's mantle. *Geochimica et Cosmochimica Acta* **56**, 1001–12.

NEUMANN, E. R., WULFF-PEDERSEN, E. & SIMONSEN, S. L. 1999. Evidence for Fractional Crystallisation of Periodically Refilled Magma Chambers in Tenerife, Canary Islands. *Journal of Petrology* **40**, 1089–1123.

PARIS, R., GUILLOU, H., CARRACEDO, J. C. & PEREZ TORRADO, F. J. 2006. Volcanic and morphological evolution of La Gomera (Canary Islands), based on new K–Ar ages and magnetic stratigraphy: implications for oceanic island evolution. *Journal of the Geological Society, London* **162**, 501–12.

PEARCE, J. A. & NORRY, M. J. 1979. Petrogenetic implications of Ti, Zr, Y, and Nb variations in volcanic rocks. *Contributions to Mineralogy and Petrology* **69**, 33–47.

PRICE, R. C. & CHAPPELL, B. W. 1975. Fractional Crystallisation and the Petrology of Dunedin Volcano. *Contribution to Mineralogy and Petrology* **53**, 157–82.

SAUNDERS, A. D. & TARNEY, J. 1984. Geochemical characteristics of basaltic volcanism within back-arc basins. In *Marginal basin geology* (eds B. P. Kokelaar & M. F. Howells), pp. 59–76. Geological Society of London, Special Publication no. 16.

SIMONSEN, S. L., NEUMANN, E. R. & SEIM, K. 2000. Sr–Nd–Pb isotope and trace-element geochemistry evidence for a young HIMU source and assimilation at Tenerife (Canary Island). *Journal of Volcanology and Geothermal Research* **103**, 299–312.

SINGER, B. S. & PRINGLE, M. S. 1996. Age and duration of the Matuyama-Brunhes geomagnetic reversal from $^{40}Ar/^{39}Ar$ incremental heating analysis of lavas. *Earth and Planetary Science Letters* **139**, 47–61.

SUN, S. S. 1980. Lead isotopic study of young volcanic rocks from mid-ocean ridges, ocean islands and island arcs. *Philosophical Transactions of the Royal Society of London* **A297**, 409–45.

WALTER, T. R. & TROLL, V. R. 2003. Experiments on rift zone evolution in unstable volcanic edifices. *Journal of Volcanology and Geothermal Research* **127**, 107–20.

WEAVER, B. L. 1991. The origin of ocean island basalt end-member compositions: trace element and isotopic constrains. *Earth and Planetary Science Letters* **104**, 381–97.

WIDOM, E., GILL, J. B. & SCHMINCKE, H.-U. 1993. Syenite Nodules as a Long-Term Record of Magmatic Activity in Agua de Pao Volcano, Sao Miguel, Azores. *Journal of Petrology* **34**, 929–53.

WOLFF, J. A. 1987. Crystallisation of nepheline syenite in a subvolcanic magma system; Tenerife, Canary Islands. *Lithos* **20**, 207–23.

WOLFF, J. A., GRANDY, J. S. & LARSON, P. B. 2000. Interaction of mantle-derived magma with island crust? Trace element and oxygen isotope data from Diego Hernandez Formation, Las Cañadas, Tenerife. *Journal of Volcanology and Geothermal Research* **103**, 343–66.

ZELLMER, G., TURNER, S. & HAWKESWORTH, C. 2000. Timescales of destructive plate margin magmatism: new insights from Santorini, Aegean volcanic arc. *Earth and Planetary Science Letters* **174**, 265–81.